Journal of Materials Chemistry

Cite this: *J. Mater. Chem.*, 2011, **21**, 8129

www.rsc.org/materials

PAPER

Preparation, characterization and luminescence properties of ternary europium complexes covalently bonded to titania and mesoporous SBA-15†

Yajuan Li and Bing Yan*

Received 25th January 2011, Accepted 24th March 2011
DOI: 10.1039/c1jm10388a

A novel multifunctional precursor Ti-MAB-S15 (MAB = *meta*-aminobenzoic acid) were prepared through the reaction of the carboxylic group with titanium alkoxide, and the amino group was modified with the coupling agent 3-(triethoxysilyl)-propyl isocyanate (TEPIC) and covalently bonded to mesoporous silica SBA-15. Then, novel organic–inorganic luminescent mesoporous hybrid titania materials, designated as $Eu(Ti\text{-}MAB\text{-}S15)_2(NTA)_3$, were obtained by introducing the $Eu(NTA)_3\cdot 2H_2O$ (NTA = 1-(2-naphthoyl)-3,3,3-trifluoroacetonate) complex into the hybrid materials Ti-MAB-S15 *via* a ligand exchange reaction. FTIR, SAXRD, N_2 absorption measurements, TEM, SEM, and photoluminescent spectra were characterized, and the results reveal that it has high surface area, is uniform in the mesostructure, and has good crystallinity. In addition, compared to the pure complex $Eu(NTA)_3\cdot 2H_2O$, the mesoporous hybrid titania material $Eu(Ti\text{-}MAB\text{-}S15)_2(NTA)_3$ exhibits longer luminescent lifetime and higher quantum efficiency, which indicates that the introduction of the multifunctional ligand Ti-MAB-S15 can sensitize the luminescence emission of the Eu^{3+} ions. Moreover, the luminescent mesoporous hybrid titania materials containing terbium ions, designated as $Tb(Ti\text{-}MAB\text{-}S15)_2(NTA)_3$, were also prepared, and were found to emit green photoluminescence characteristic of terbium ions.

1. Introduction

It is well known that lanthanide complexes have a variety of potential technological applications, such as in fluoroimmunoassays, optical amplification, light-conversion molecular devices and organic light-emitting devices.[1] This is mainly because they exhibit high luminescence quantum efficiency, sharp and intense emission lines, long lifetimes and high color purity upon ultraviolet light irradiation, through the effective intramolecular energy transfer from the coordinated ligands to the luminescent central lanthanide ions (the so-called "antenna affect").[2] However, they have so far been excluded from practical applications as optical devices mainly due to their poor thermal stabilities and low mechanical strength. One solution is to immobilize the complexes in stable rigid matrixes, for example, polymer,[3] liquid crystal,[4] or silica-based materials.[5] In the past few years, ordered mesoporous silicas used as a support for lanthanide complexes have attracted much attention.[6] Most of the earlier studies were mainly focused on doping mesoporous silica materials with lanthanide complexes, in which only weak physical interactions (typically hydrogen bonding, van der Waals forces, or weak static effects) exist between the mesoporous silica materials and the lanthanide complexes. This will give little control over the quenching effect of emitting centers, inhomogeneous dispersion of both phases, and leaching of the photoactive molecules. Therefore, another appealing method in regard to complexation of lanthanide ions using ligands that are covalently bonded to the mesoporous silica network has emerged, and the as-derived molecular-based materials exhibit a higher and more homogeneous surface coverage of organosilane functionalities and improved luminescent properties. In addition, among all mesoporous materials, SBA-15 has certainly become one of the most attractive hosts owing to its high hydrothermal stability and the presence of hexagonally ordered large mesopores (*P6mm* symmetry group) interconnected by complementary micropores.[7] Recently, Zhang[8] and our group[9] have done several studies on the synthesis and photoluminescence properties studies of lanthanide complexes covalently bonded to mesoporous SBA-15. It is shown that promising visible-luminescent properties can be obtained by linking the lanthanide complexes to mesoporous materials.

On the other hand, titania has started to attract much attention as a host matrix for lanthanide complexes because of its peculiar and fascinating physicochemical properties and a wide variety of potential uses in diverse fields, including solar cells, energy conversion, environmental purification, and photocatalysis.[10] Recently, Li and co-workers reported a novel method

Department of Chemistry, Tongji University, Siping Road 1239, Shanghai, 200092, China. E-mail: byan@tongji.edu.cn; Fax: +86-21-65982287; Tel: +86-21-65984663

† Electronic supplementary information (ESI) available. See DOI: 10.1039/c1jm10388a

to immobilize lanthanide complexes on titania *via* modification of the titanium alkoxide, and the as-derived materials exhibit excellent photoluminescence properties.[11]

Taking into account the above, it would be highly attractive to investigate the luminescence properties of lanthanide mesoporous complexes grafted to titania, which not only will result in systems with interesting properties but also is a key study on the chemical possibilities to tether metal complexes to mesoporous silica and nonsilicate metal oxides simultaneously. To the best of our knowledge, the research on this regard has not been reported so far. In the present paper, we present a novel method to tether lanthanide mesoporous materials to titania by employing *meta*-aminobenzoic acid. This compound has a double function: (1) the carboxylic acid group can react with titanium alkoxide to moderate the reactivity towards hydrolysis and condensation; (2) the amino group can be modified with TESPIC and covalently bonded to mesoporous silica, and then coordinated to lanthanide ions. In addition, in order to improve the photoluminescence properties of the lanthanide materials, we have introduced 1-(2-naphthoyl)-3,3,3-trifluoroacetonate (NTA) to coordinate with the lanthanide ions because the ligand NTA can act both as an antenna to absorb and transfer energy to the metal ions and to expel water molecules from the first coordination sphere.[12]

2. Experimental section

Chemicals and procedures

Reagents. Tetraethoxysilane (TEOS), 1-(2-naphthoyl)-3,3,3-trifluoroacetonate (NTA), 3-(triethoxysilyl)-propyl isocyanate (TEPIC), triblock copolymer poly(ethylene glycol)-*block*-poly (propylene glycol)-*block*-poly-(ethylene glycol) (Pluronic P123, $EO_{20}PO_{70}EO_{20}$), *meta*-aminobenzoic acid (MAB), tetraisopropyl titanate ($Ti(OCH(CH_3)_2)_4$) and tetraethoxysilane (TEOS) were purchased from Aldrich and used without further purification. Terbium and europium nitrate were obtained by dissolving their respective oxides (Tb_4O_7 and Eu_2O_3) in concentrated nitric acid. The other chemicals were all commercially available and used as received.

Synthesis of cross-linking precursor containing Si–O chemical bonds (MAB-Si). A typical procedure for the preparation of the modified precursor MAB-Si was as follows: 1.0 mmol MAB was firstly dissolved in 20 mL of $CHCl_3$. 1.0 mmol (0.25 g) of TEPIC was add dropwise into the solution with stirring. The mixture was heated at 70 °C in a covered flask for approximately 10 h under a nitrogen atmosphere. Then cold hexane was added to precipitate the white powder. The powder was obtained by filtration, purified in hexane and dried in a vacuum. ^{1}H NMR ($CDCl_3$, 400 MHz): d 1.24 (18H, m), 3.73 (m, 12H), 0.64 (4H, t), 1.83 (4H, m), 3.82 (4H, t), 8.63 (1H, s), 6.98 (1H, d), 7.90 (1H, m), 7.75 (1H, d). Therefore, we could infer that the precursor MAB-Si has been synthesized successfully as proved by the data.

Synthesis of *meta*-aminobenzoic acid-functionalized SBA-15 material (MAB-S15). MAB-functionalized SBA-15 mesoporous material was synthesized from an acidic mixture with the following molar composition: 0.0172 P123 : 0.96 TEOS : 0.04 MAB-Si : 6 HCl : 208.33 H_2O. P123 (1.0 g) was dissolved in deionized water (7.5g) and 2 M HCl solution (30 g) at 35 °C. A mixture of MAB-Si and TEOS was added into the above solution at 35 °C with stirring for 24 h and transferred into a Teflon bottle sealed in an autoclave, which was heated at 100 °C for 48 h. Then the solid product was filtered, washed thoroughly with deionized water, and air-dried for 12 h at 60 °C. Removal of copolymer surfactant P123 was conducted by Soxhlet extraction with ethanol under reflux for 2 days to give the sample denoted as MAB-S15.

Synthesis of organic ligand grafted onto mesoporous silica matrix and Ti–O network simultaneously (Ti-MAB-S15). The mesoporous material MAB-S15 was soaked in ethanol with stirring and an equimolar amount of $Ti(OCH(CH_3)_2)_4$ was added into the solution. The mixture was refluxing at 65 °C for 3 h, followed by filtration and extensive washing with EtOH. After drying in a vacuum at 65 °C for 10 h, the solid hybrid material Ti-MAB-S15 was obtained.

Synthesis of the lanthanide complexes $Ln(NTA)_3\cdot 2H_2O$ (Ln = Eu, Tb). $Ln(NTA)_3\cdot 2H_2O$ complexes were prepared for Ln = Eu, Tb, according to the published procedure as described below.[13] Under stirring, 1 mmol of $Ln(NO_3)_3\cdot 6H_2O$ ethanol solution was added dropwise to a solution of NTA (3 mmol) in ethanol (20 mL) that has been neutralized with 3 mmol sodium hydroxide. The mixture was heated to 80 °C for 4 h, then filtered, washed with ethanol, and finally dried in a vacuum overnight. The purity of the compounds was verified by CHN elemental analysis.

Synthesis of ternary hybrid materials containing Ti–O network and mesoporous silica network ($Ln(Ti\text{-}MAB\text{-}S15)_2(NTA)_3$, Ln = Eu, Tb). The Ti-MAB-S15-derived hybrid material was prepared as follows. Firstly, the mesoporous material Ti-MAB-S15 was soaked in ethanol with stirring at 65 °C for 3 h, then an appropriate amount of $Ln(NTA)_3\cdot 2H_2O$ ethanol solution (molar ratio of Ti-MAB-S15 : $Ln(NTA)_3\cdot 2H_2O$ = 2 : 1) was added dropwise into the above solution, and an appropriate amount of H_2O was added. The stirring was continued for another 24 h to yield a precipitate, which was recovered by filtration and extensive washing with EtOH. The resulting material $Ln(Ti\text{-}MAB\text{-}S15)_2(NTA)_3$ was dried at 65 °C under vacuum overnight. The detailed synthesis process and the predicted structure of $Eu(Ti\text{-}MAB\text{-}S15)_2(NTA)_3$ are outlined in Scheme 1.

Synthesis of binary hybrid materials containing Ti–O network and mesoporous silica network ($Eu(Ti\text{-}MAB\text{-}S15)_4$). The synthesis procedure of the hybrid material $Eu(Ti\text{-}MAB\text{-}S15)_4$ was similar to that of $Eu(Ti\text{-}MAB\text{-}S15)_2(NTA)_3$ except that Eu $(NTA)_3\cdot 2H_2O$ ethanol solution was replaced by Eu $(NO_3)_3\cdot 6H_2O$ ethanol solution, and the molar ratio of Ti-MAB-S15 : $Eu(NO_3)_3\cdot 6H_2O$ = 4 : 1. The predicted structure of $Eu(Ti\text{-}MAB\text{-}S15)_4$ was obtained and is outlined in Scheme S1.†

Physical measurements

^{1}H NMR spectra were recorded in $CDCl_3$ on a BRUKER AVANCE-400 spectrometer with tetramethylsilane (TMS) as internal reference. FTIR spectra were measured within the 4000–400 cm^{-1} region on an Nicolet model 5SXC FT-IR spectrophotometer with the KBr pellet technique. The ultraviolet

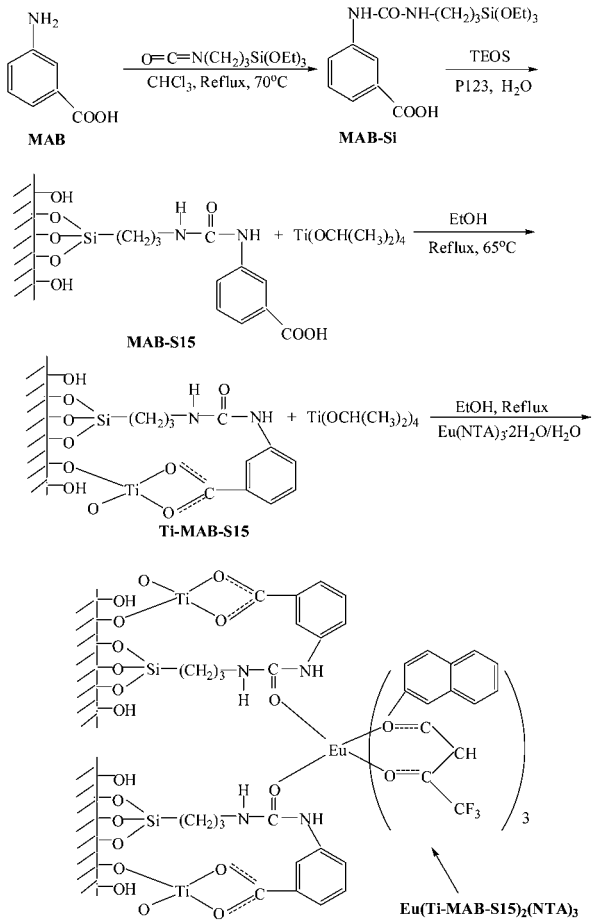

Scheme 1 Synthesis procedure and predicted structure of the ternary mesoporous hybrid titania materials $Eu(Ti\text{-}MAB\text{-}S15)_2(NTA)_3$.

absorption spectra were taken with an Agilent 8453 spectrophotometer. The X-ray diffraction (XRD) measurements were carried out using powder samples *via* a BRUKER D8 diffractometer (40 mA/40 kV), using monochromated Cu-Kα_1 radiation (λ = 1.54 Å) in a 2θ range from 0.6° to 6°. Nitrogen adsorption/desorption isotherms were measured at the liquid nitrogen temperature, using a Nova 1000 analyzer. The samples were outgassed for 3 h at 150 °C before the measurements. Surface areas were calculated by the Brunauer–Emmett–Teller (BET) method and pore size distributions were evaluated from the desorption branches of the nitrogen isotherms using the Barrett–Joyner–Halenda (BJH) model. The fluorescence excitation and emission spectra were obtained on a SHIMADZU RF-5301 spectrophotometer. Luminescence lifetime measurements were determined on an Edinburgh Instrument FLS920 phosphorimeter using a 450 W xenon lamp as the excitation source (pulse width, 3 μs). Scanning electronic microscopy (SEM) was performed on a Philips XL-30. Transmission electron microscope (TEM) experiments were conducted on a JEOL2011 microscope operated at 200 kV or on a JEM-4000EX microscope operated at 400 kV.

3. Results and discussion

A novel organic-inorganic mesoporous hybrid titania materials $Eu(Ti\text{-}MAB\text{-}S15)_2(NTA)_3$ was prepared *via* a ligand exchange reaction, and the synthesis process and the predicted structure of this hybrid are shown in Scheme 1. Generally it is very difficult to prove the exact structure of this kind of non-crystalline hybrid material and it is hardly possible to solve the coordination behaviour of lanthanide ions. However, the main composition and coordination effect according to the lanthanide coordination chemistry principle and the configuration of the organic functional groups can be predicted. The rare earth positive ions are hard Lewis acids so they readily coordinate with hard bases containing oxygen and nitrogen atoms. Additionally, most of the lanthanide complexes hold polar covalent bonds as the lanthanide ions always bond through the 6s, 6p, and 5d electronic orbitals, whose electron count is nine. Therefore, it is most stable for the lanthanide complex to exist with the coordination number of eight or nine. Furthermore, in our experiment we synthesize the material by adding the appropriate and accurate proportion of reagent into the system [Ti-MAB-S15 : $Ln(NTA)_3 \cdot 2H_2O$ = 2 : 1] to obtain the fixed model of lanthanide complex. Furthermore, in view of the spatial steric hindrance effect, we predicted the optimum coordination structure for the hybrid material.

The selection of the ligand is the key point for the preparation of this hybrid material. Herein, the organic ligand MAB is selected as a multifunctional linker, which not only can be covalently bonded to the framework of mesoporous silica and coordinate to lanthanide ions as well as sensitize the luminescence of them, but also can modify the reactivity of the titanium precursor and introduce titania matrix to the hybrid system. The infrared spectra of MAB (A), MAB-Si (B), MAB-S15 (C), and Ti-MAB-S15 (D) are shown in Fig. 1. From A to B, it can be observed that there are new bands located at 2970, 2925, and 2886 cm^{-1}, which originated from the three methylene groups of TEPIC. In addition, the spectrum of MAB-Si is dominated by ν(C–Si, 1168 cm^{-1}) and ν(C–Si, 1080 cm^{-1}) absorption bands, characteristic of trialkoxylsilyl functions, and the band centered at 3420 cm^{-1} corresponds to the stretching vibration of grafted –NH– groups and the hydroxyl groups of adsorbed water together in B. Moreover, the bending vibration (δ_{NH}, 1564 cm^{-1}) further proves the formation of amide groups. New peaks at 1640 cm^{-1} in B were attributed to the absorptions of the –CONH

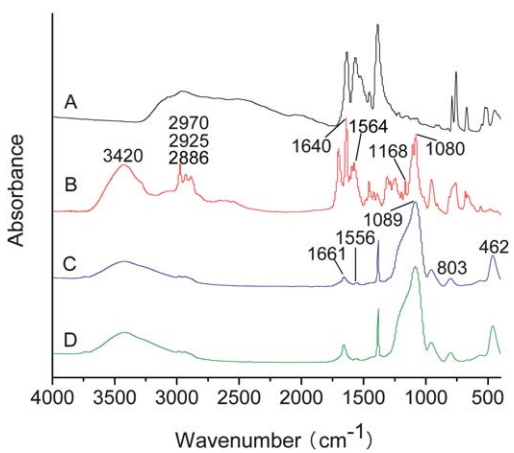

Fig. 1 The infrared spectra of MAB (A), MAB-Si (B), MAB-S15 (C), and Ti-MAB-S15 (D).

group deriving from the cross-linking reagent TEPIC, proving that TEPIC was successfully grafted onto the ligand MAB.[14] It is worth noting that the bands at 1661 and 1556 cm^{-1} ascribed to the vibrations of NH–CO–NH can be also observed in Fig. 1(C), suggesting that MAB-Si was successfully incorporated into the mesoporous silica SBA-15. Furthermore, the formation of a Si–O–Si framework is clearly evidenced by the broad bands located at 1089 cm^{-1} (ν_{as}, Si–O–Si), 803 cm^{-1} (ν_s, Si–O–Si), and 462 cm^{-1} (δ, Si–O–Si). The spectrum of Ti-MAB-S15 (D) is similar to that of C, and the characteristic absorption of Ti–O is not clearly shown in the spectrum, which is mainly attributed to the lower content in the material or the shielding effect of the host material.

The small-angle X-ray diffraction (SAXRD) patterns and nitrogen adsorption/desorption isotherms are popular and efficient methods to characterize highly ordered mesoporous material with hexagonal symmetry of the space group *p6mm*. Fig. 2 presents the SAXRD patterns of a pure SBA-15 mesoporous silica (A), Eu(Ti-MAB-S15)$_4$ (B), Eu(Ti-MAB-S15)$_2$(NTA)$_3$ (C), and Tb(Ti-MAB-S15)$_2$(NTA)$_3$ (D). The pure SBA-15 mesoporous silica exhibits three characteristic reflections in the 2θ range of 0.6–6°, which are indexed as (100), (110) and (200) diffractions of the hexagonal mesostructure. As shown in Fig. 2, the Bragg peaks indexed as (100) are observed in the lanthanide hybrid material (B–D), which suggests the ordered hexagonal mesoporous structure of SBA-15 are substantially conserved after the introduction of the lanthanide complex. However, it is worth noting that the intensities of these hybrid material Bragg peaks are reduced to the extent that the (110) and (200) reflection are either absent or very weak. This can be attributed to the decrease of structure ordering degree which might be due to the reduction of scattering contrast between the channel walls of the matrices and the covalently bonded lanthanide complexes in the mesoporous materials.[15] Meanwhile, the hexagonal mesostructure of Eu(Ti-MAB-S15)$_2$(NTA)$_3$ is further confirmed by TEM micrographs (see Fig. 3). As shown in the figure, the hybrid material Eu(Ti-MAB-S15)$_2$(NTA)$_3$ exhibits a regular hexagonal array of uniform channels, which suggests that the mesostructure of the resulting material can substantially be conserved after the modification with Ti–O network and complexation process,

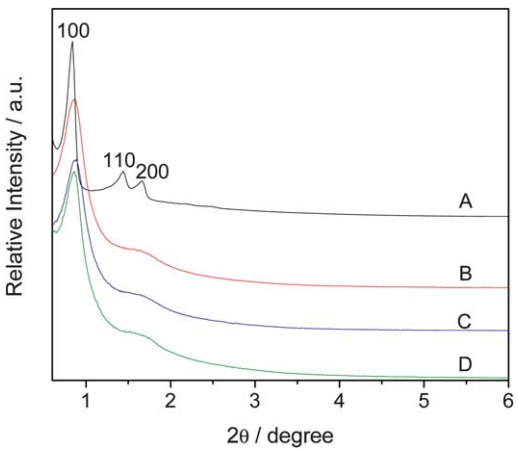

Fig. 2 SAXRD patterns of pure SBA-15 mesoporous silica (A), Eu(Ti-MAB-S15)$_4$ (B), Eu(Ti-MAB-S15)$_2$(NTA)$_3$ (C), and Tb(Ti-MAB-S15)$_2$(NTA)$_3$ (D).

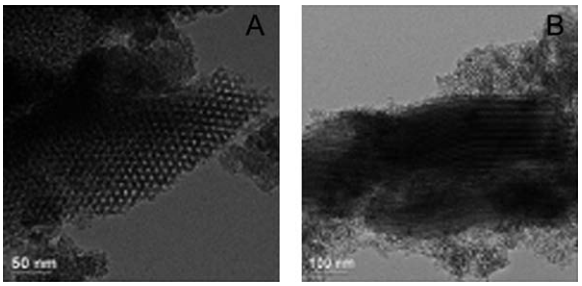

Fig. 3 TEM images of Eu(Ti-MAB-S15)$_2$(NTA)$_3$ recorded along the [100] (A) and [110] (B) zone axes.

coincident with the results of XRD patterns. The distance between the centers of the mesopores is estimated to be around 11 nm, which is in good agreement with the value determined from the corresponding XRD analysis (see Table 1).

The N_2 adsorption–desorption isotherms for pure SBA-15 (A), Eu(Ti-MAB-S15)$_4$ (B), Eu(Ti-MAB-S15)$_2$(NTA)$_3$ (C), and Tb(Ti-MAB-S15)$_2$(NTA)$_3$ (D) are shown in Fig. 4. They all display Type IV isotherms with H1-type hysteresis loops at high relative pressure according to the IUPAC classification,[16] characteristic of mesoporous materials with highly uniform size distributions. The specific area and the pore size have been calculated by using Brunauer–Emmett–Teller (BET) and Barrett–Joyner–Halenda (BJH) methods, respectively. The structure data of all these mesoporous materials (BET surface area, total pore volume, pore size, *etc.*) are summarized in Table 1. It can be clearly seen that pure SBA-15 has a high BET surface area (1197 $m^2\ g^{-1}$), a large pore volume (1.81 $cm^3\ g^{-1}$), and a BJH pore diameter of 7.39 nm, indicative of its potential application as a host in luminescent materials. It is obvious that the surface areas, pore volumes and pore diameters of the lanthanide hybrid materials decrease after immobilization of lanthanide complexes into SBA-15, suggesting that the complexes are grafted inside the mesopores.[15]

A scanning electron micrograph of mesoporous hybrid material Eu(Ti-MAB-S15)$_4$(NTA)$_3$ is shown in Fig. 5. It can be observed that the sample consists of relatively uniform globe-like particles. It demonstrates that a homogeneous, molecular-based material was obtained because of strong covalent bonds between the organic ligand MAB and the inorganic mesoporous silica and titania matrix, and the coordinate bonds between organic ligand β-diketone or mesoporous hybrid material containing Ti–O network (Ti-MAB-S15) and rare earth ions, which belong to a complicated huge molecular system in nature. Compared with the hybrid materials with doped lanthanide complexes generally experiencing phase separation phenomena, in this paper, the inorganic and organic phases can exhibit their distinct properties together in the hybrid materials we obtained containing covalent bonds.

The fluorescence excitation and emission spectra of the resulting ternary europium mesoporous hybrid titania material Eu(Ti-MAB-S15)$_2$(NTA)$_3$, binary europium mesoporous hybrid titania material Eu(Ti-MAB-S15)$_4$, and pure complex Eu(NTA)$_3$·2H_2O, are displayed in Fig. 6a and b, respectively (A for Eu(NTA)$_3$·2H_2O, B for Eu(Ti-MAB-S15)$_2$(NTA)$_3$, and C for Eu(Ti-MAB-S15)$_4$). The normalized excitation spectra of these

Table 1 Structural parameters of SBA-15, Eu(Ti-MAB-S15)$_4$, Eu(Ti-MAB-S15)$_2$(NTA)$_3$, and Eu(Ti-MAB-S15)$_2$(NTA)$_3$[a]

Sample	d_{100}/nm	a_0/nm	S_{BET}/m^2 g^{-1}	V/cm^3 g^{-1}	D/nm
SBA-15	10.76	12.42	1197	1.81	7.39
Eu(Ti-MAB-S15)$_4$	10.90	11.71	572	0.97	5.68
Eu(Ti-MAB-S15)$_2$(NTA)$_3$	10.64	11.82	546	0.92	5.56
Tb(Ti-MAB-S15)$_2$(NTA)$_3$	10.64	11.82	597	0.94	5.30

[a] d_{100} is the d(100) spacing, a_0 the cell parameter ($a_0 = 2\ d_{100}/\sqrt{3}$), S_{BET} the BET surface area, V the total pore volume, D_{BJH} the average pore diameter.

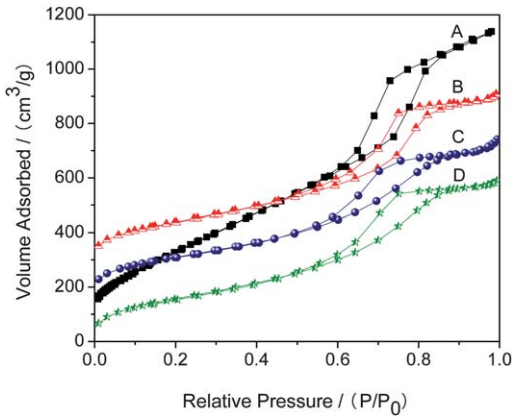

Fig. 4 N_2 adsorption–desorption isotherms for pure SBA-15 mesoporous silica (A), Eu(Ti-MAB-S15)$_4$ (B), Eu(Ti-MAB-S15)$_2$(NTA)$_3$ (C), and Tb(Ti-MAB-S15)$_2$(NTA)$_3$ (D).

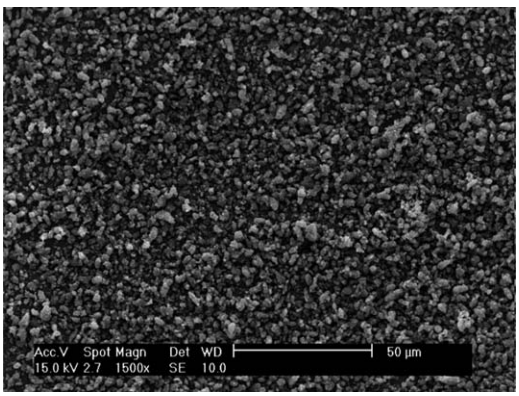

Fig. 5 SEM image of mesoporous ternary hybrid titania material Eu(Ti-MAB-S15)$_2$(NTA)$_3$.

materials were obtained by monitoring at the $^5D_0 \rightarrow {}^7F_2$ emission lines (614 nm). As shown in Fig. 6a, the excitation spectrum of the pure Eu(NTA)$_3\cdot 2H_2O$ complex exhibits a broad excitation band between 220 and 450 nm (λ_{max} = 380 nm), which can be assigned to the π–π^* states of the organic ligand.[17] Compared with the pure complex Eu(NTA)$_3\cdot 2H_2O$, the excitation band of the mesoporous hybrid material Eu(Ti-MAB-S15)$_2$(NTA)$_3$ becomes narrower and the maximum excitation wavelength shifted from 380 nm to 342 nm. The blue shift of the excitation bands upon introduction of organic ligands with Ti–O network and mesoporous silica into the pure complex is due to a hypsochromic effect resulting from the change in the polarity of the environment surrounding the europium complex in the mesoporous hybrid material.[18] For europium binary mesoporous hybrid Eu(Ti-MAB-S15)$_4$, the excitation is dominated by a broad band and a narrow peak centered at 393 nm, the former band is attributed to the absorption of the organic ligand and the latter narrow peak is ascribed to the absorption transition ($^7F_0 \rightarrow {}^5L_6$) of the f–f transition of Eu^{3+}. The f–f transition is weaker than the absorption of the organic ligand, which indicates that luminescence sensitization *via* the excitation of the ligand is much more efficient than the direct excitation of the Eu^{3+} ion absorption level. For europium ternary mesoporous hybrid Eu(Ti-MAB-S15)$_2$(NTA)$_3$, the non-observation of Eu^{3+} intra-4f^6 lines indicates that the energy transfer from the ligands to

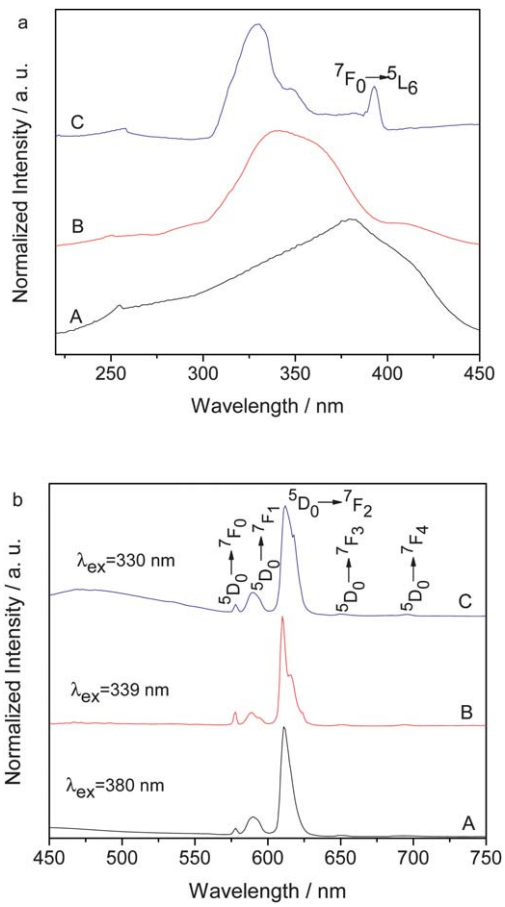

Fig. 6 Room temperature excitation (a) and emission (b) spectra of (A) pure complex Eu(NTA)$_3\cdot 2H_2O$, (B) ternary europium mesoporous hybrid titania material Eu(Ti-MAB-S15)$_2$(NTA)$_3$, and (C) binary europium mesoporous hybrid titania material (Ti-MAB-S15)$_4$. All spectra are normalized to a constant intensity at the maximum.

Eu^{3+} ion is more efficient in $Eu(Ti\text{-}MAB\text{-}S15)_2(NTA)_3$ than in the binary hybrid $Eu(Ti\text{-}MAB\text{-}S15)_4$.

Fig. 6b shows the normalized emission spectra for the obtained Eu^{3+}-containing materials as solids at room temperature. They all reveal the characteristic emission bands of Eu^{3+} ion centered at about 577, 589, 612, 650 and 696 nm, corresponding to the $^5D_0 \rightarrow {}^7F_J$ transitions ($J = 0$, 1, 2, 3 and 4, respectively). Among these transitions, the $^5D_0 \rightarrow {}^7F_2$ transition at about 612 nm shows the most prominent emission. It is well known that $^5D_0 \rightarrow {}^7F_2$ belongs to a typical electric dipolar transition and strongly varies with the local symmetry of Eu^{3+} ions, whereas the $^5D_0 \rightarrow {}^7F_1$ transition is a parity-allowed magnetic dipolar transition, which is independent of the host material. Therefore, the relative intensity ratio (R_I) of $^5D_0 \rightarrow {}^7F_2$ to $^5D_0 \rightarrow {}^7F_1$ is sensitive to the symmetry around the Eu^{3+} ion and gives valuable information about the chemical microenvironment change of anions coordinating the Eu^{3+} ion.[19] The R_I values for three kinds of materials are listed in Table 2. By comparison, it can be observed that the R_I value of mesoporous hybrid $Eu(Ti\text{-}MAB\text{-}S15)_2(NTA)_3$ (7.8) is much higher than that of $Eu(NTA)_3\cdot 2H_2O$ (5.4), which suggests the introduction of organic ligand Ti-MAB-S15 into the complex may make the material have high polarity, which may affect the centrosymmetric environment of the Eu^{3+} ions, and thus influence the R_I value.

The luminescence lifetimes and quantum yields, which are two important parameters for the estimation of the efficiency of the emission process of the complexes, have also been determined. The decay lifetime values of $^5D_0$ excited states were measured at room temperature under the excitation wavelength that maximizes the emission intensity and monitored by the most intense emission line at 613 nm. The luminescence decay curve of the ternary mesoporous hybrid titania material $Eu(Ti\text{-}MAB\text{-}S15)_2(NTA)_3$ is shown in Fig. 7, and the decay curves of materials $Eu(NTA)_3\cdot 2H_2O$ and $Eu(Ti\text{-}MAB\text{-}S15)_4$ are also given in the ESI (Fig. S1(A) and (B)†). The lifetime profiles for three samples are fitted with single exponentials, demonstrating that all the Eu^{3+} ions are located in the same local environment in the obtained hybrid materials. The resulting lifetimes (shown in Table 2) are on the same order of magnitude for all samples. On the basis of the emission spectra and lifetimes of the $^5D_0$ emitting level, the emission quantum efficiency (η) of the $^5D_0$ europium ion excited state can be determined. Assuming that only

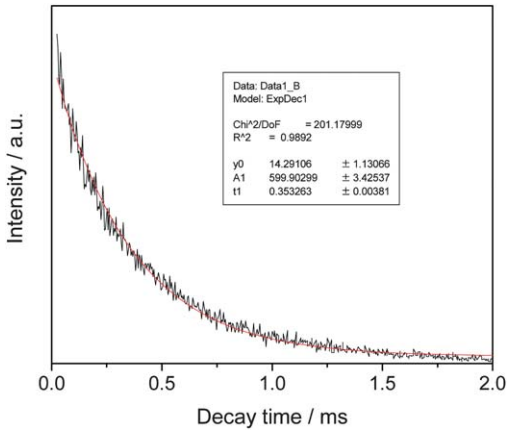

Fig. 7 Luminescence decay curve of the ternary mesoporous hybrid titania material $Eu(Ti\text{-}MAB\text{-}S15)_2(NTA)_3$.

nonradiative and radiative processes are essentially involved in the depopulation of the $^5D_0$ state, η can be expressed as:[20]

$$\eta = A_r/(A_r + A_{nr}) \quad (1)$$

Here, A_r and A_{nr} are radiative and nonradiative transition rates, respectively. A_r can be obtained by summing over the radiative rates A_{0J} for each $^5D_0 \rightarrow {}^7F_J$ ($J = 0$–4) transitions (the $^5D_0 \rightarrow {}^7F_{5,6}$ branching ratios are neglected due to their poor relative intensity with respect to that of the remaining $^5D_0 \rightarrow {}^7F_{0-4}$ lines). The $^5D_0 \rightarrow {}^7F_1$ transition does not depend on the local ligand field and thus may be used as a reference for the whole spectrum. An effective refractive index of 1.5 was used leading to $A_{01} \approx 50\ s^{-1}$,[21] where A_{01} stands for the Einstein's coefficient of spontaneous emission between the $^5D_0$ and the $^7F_1$ Stark levels. The lifetime, radiative (A_r), and nonradiative (A_{nr}) transition rates are related through the following equation:

$$\tau_{exp} = (A_r + A_{nr})^{-1} \quad (2)$$

On the basis of the above discussion, the parameters A_r, A_{nr} and the quantum efficiency values, η, for the $^5D_0$ Eu^{3+} ion excited state in the three materials can be obtained, as shown in Table 2. According to the relationship between the quantum efficiency radiative and nonradiative transition rates, it can be found the

Table 2 Photoluminescence data of $Eu(NTA)_3\cdot 2H_2O$, $Eu(Ti\text{-}MAB\text{-}S15)_2(NTA)_3$, and $Eu(Ti\text{-}MAB\text{-}S15)_4$ as solids[a]

	$Eu(NTA)_3\cdot 2H_2O$	$Eu(Ti\text{-}MAB\text{-}S15)_2(NTA)_3$	$Eu(Ti\text{-}MAB\text{-}S15)_4$
R	5.4	7.8	4.7
t (ms)[c]	0.353 ± 0.004	0.464 ± 0.002	0.306 ± 0.004
$t^{-1}(s^{-1})$	2833	2155	3268
A_r (s^{-1})	360	531	328
A_{nr} (s^{-1})	2473	1624	2940
η (%)	12.7	24.6	10.0
n_w	2.3	1.4	2.9
Ω_2 ($\times 10^{-20}$ cm^2)	8.9	12.6	7.7
Ω_4 ($\times 10^{-20}$ cm^2)	0.31	0.70	0.31

[a] R_I, intensity ratios of $^5D_0 \rightarrow {}^7F_2$ to $^5D_0 \rightarrow {}^7F_1$; t, decay time; A_r, radiative decay rates; A_{nr}, nonradiative decay rates; h, the emission quantum efficiency of the $^5D_0$ Eu^{3+} excited state calculated from the decay time and the emission intensities; n_w, the number of water molecules coordinated to the Eu^{3+} ion; Ω_λ, the experimental intensity parameters.

value h mainly depends on the values of two factors: one is lifetime and the other is relative intensity ratio R (I_{02}/I_{01}). As we can see from Table 2, hybrid material Eu(Ti-MAB-S15)$_2$(NTA)$_3$ exhibits longer lifetime and higher R value than that of pure complex Eu(NTA)$_3\cdot$2H$_2$O, so the quantum efficiency of hybrid Eu(Ti-MAB-S15)$_2$(NTA)$_3$ (24.6%) is much higher than that of Eu(NTA)$_3\cdot$2H$_2$O (12.7%). This is mainly because the carbonyl oxygen atoms located in the organic ligand Ti-MAB-S15 coordinated to Eu^{3+} ions could replace the water molecules from the first coordination sphere of europium ions, the energy loss and clustering of the emitting centers caused by the vibration of the hydroxyl groups of coordinated water molecules could be avoided. It is also worth noting that compared with binary mesoporous hybrid Eu(Ti-MAB-S15)$_4$ (10.0%), the quantum efficiency of ternary mesoporous hybrid Eu(Ti-MAB-S15)$_2$(NTA)$_3$ (24.6%) exhibits obvious enhancement, which is the main reason why the presence of β-diketonate ligands can shield the europium ions from water molecules and can help to absorb the excitation energy and to transfer it to the central metal ions.[22]

In order to elucidate the negative influence of vibration caused by the water molecules and further study the coordination environment surrounding the rare earth ions in the mesoporous hybrid materials, we further selectively estimated the number of coordination molecules for Eu hybrid material systems. The number of water molecules coordinated to the Eu^{3+} ions (n_w) can be determined with the empirical formula reported by Supkowski and Horrocks:[23]

$$n_w = 1.11 \times (\tau^{-1} - A_r - 0.31) \quad (3)$$

All the calculated results are shown in Table 2. Based on the results, the coordination numbers of water molecules in materials Eu(NTA)$_3\cdot$2H$_2$O, Eu(Ti-MAB-S15)$_4$, and Eu(Ti-MAB-S15)$_2$(NTA)$_3$ are 2.3, 1.4, and 2.9, respectively. The water molecules produce the severe vibration of hydroxyl group, resulting in the large non-radiative transition and decreasing the luminescent efficiency.

Moreover, the experimental intensity parameters (Ω_λ, $\lambda = 2$ and 4) for the europium material can be calculated by the method originally proposed by Krupke[24] and subsequently used by others.[25] This method takes advantage of the fact that the emission intensities of the $^5D_0 \rightarrow {}^7F_2$, $^5D_0 \rightarrow {}^7F_4$, and $^5D_0 \rightarrow {}^7F_6$ transitions are solely dependent on the Ω_2, Ω_4, and Ω_6 parameters, respectively. The radiative transition rate of $^5D_0 \rightarrow {}^7F_1$, which possesses solely magnetic dipole character and is insensitive to the site symmetry, is used as a reference to scale the absolute ED transition rates of $^5D_0 \rightarrow {}^7F_J$ ($J = 2$, 4, 6) by the equation:[25]

$$A_{MD}(J \rightarrow J') = (64\pi^4 e^2 n^3 \upsilon^3)/[3h(2J+1)](e\hbar/2mc)^2 |\langle \Phi J \| L + 2S \| \Phi' J' \rangle|^2 \quad (4)$$

where e is electronic charge; n is the effective index of refraction, as will be mentioned in the luminescence quantum yield section ($n = 1.5$); υ is the average transition energy in cm^{-1}; $|\langle \Phi J \| L + 2S \| \Phi' J' \rangle|^2$ are the reduced matrix elements (RME) of the MD operator, which were calculated based on the intermediate-coupling wave functions. Once the ED radiative transition rates of $^5D_0 \rightarrow {}^7F_J$ ($J = 2$, 4, 6) are determined, the experimental intensity parameters (Ω_λ, $\lambda = 2$, 4, 6) can be calculated using the following formula:[25,26]

$$A_{ED}(J \rightarrow J') = [(64\pi^4 e^2 \upsilon^3)/3h(2J+1)]\{[n(n^2+2)^2/9] \Sigma \Omega_\lambda |\langle \Phi J \| U^{(\lambda)} \| \Phi' J' \rangle|^2 \quad (5)$$

where $|\langle \Phi J \| U^{(\lambda)} \| \Phi' J' \rangle|^2$ are the RMEs of the unit tensor. The $^5D_0 \rightarrow {}^7F_6$ transition could not be experimentally detected and it is not necessary to determine its experimental intensity parameters. According to the emission spectra (Fig. 6), the experimental intensity parameters Ω_2, Ω_4 were determined and are listed in Table 2. It can be observed that the ternary hybrid mesoporous titania material Eu(Ti-MAB-S15)$_3$(NTA)$_2$ possesses a relative high value of the Ω_2 intensity parameter, which may be interpreted as a consequence of the hypersensitive behavior of the $^5D_0 \rightarrow {}^7F_2$ transition. The dynamic coupling mechanism is, therefore, dominant, indicating that the Eu^{3+} ion is in a highly polarizable chemical environment and suggesting an improvement of the luminescence in Eu(Ti-MAB-S15)$_3$(NTA)$_2$ when compared with that exhibited by the Eu(NTA)$_3\cdot$2H$_2$O complex.[8]

Furthermore, the europium(III) ions can be replaced in this system by other lanthanide ions that show luminescence with different colors. The hybrid material Tb(Ti-MAB-S15)$_2$(NTA)$_3$, which shows green photoluminescence upon radiation with ultraviolet light (254 nm and 365 nm), was also obtained. The normalized excitation and emission spectra of the hybrid Tb(Ti-MAB-S15)$_2$(NTA)$_3$ are shown in Fig. 8. The excitation spectrum of the material was obtained by monitoring the emission of the Tb^{3+} ions at 545 nm. The spectrum presents a broad band ranging from 250 nm to 400 nm with the maximum intensity at 350 nm, which is due to the characteristic absorption of the organic ligands, and no f–f transitions could be observed. This indicates that an effective energy transfer occurs from the ligands to the central Tb^{3+} ions. Excitation at 350 nm provides the typical luminescence of Tb^{3+} ion at 488, 543, 583, and 620 nm, corresponding to $^5D_4 \rightarrow {}^7F_J$ transitions ($J = 6$, 5, 4 and 3, respectively). The typical green color of terbium emission is mostly ascribed to the strongest transition ($^5D_4 \rightarrow {}^7F_5$) centered at 545 nm.

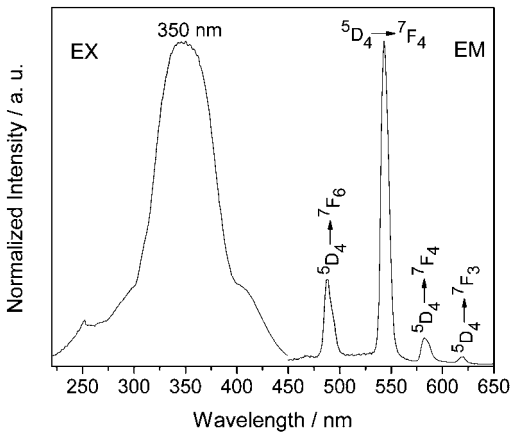

Fig. 8 Room temperature excitation spectra (left) and emission spectra of ternary terbium mesoporous hybrid titania material Tb(Ti-MAB-S15)$_2$(NTA)$_3$ (right). Both spectra are normalized to a constant intensity at the maximum.

4. Conclusions

In summary, ternary europium luminescent mesoporous hybrid titania material Eu(Ti-MAB-S15)$_2$(NTA)$_3$ was successfully prepared by linking lanthanide complexes Eu(NTA)$_3\cdot$2H$_2$O complex to the mesoporous hybrid titania material Ti-MAB-S15 *via* a ligand exchange reaction, which provides a representative method for assembling luminescent lanthanide molecular-based hybrid materials containing ordered mesoporous Si–O network and amorphous Ti–O network simultaneously. The obtained material preserves the ordered mesoporous structures and shows highly uniform pore size distributions. Further investigation on the luminescence properties confirm that the europium mesoporous hybrid titania material Eu(Ti-MAB-S15)$_2$(NTA)$_3$ exhibits higher $^5D_0$ luminescence quantum efficiency and longer lifetime than the pure Eu(NTA)$_3\cdot$2H$_2$O complex and binary mesoporous hybrid titania material Eu(Ti-MAB-S15)$_4$. In addition, this reaction principle is not limited to europium compounds but can be extended to other lanthanide compounds that emit in the visible and near-infrared regions, thus opening a door for the development of new materials. The excellent luminescent properties of this kind of material, together with the highly ordered mesoporous structures containing Ti–O network will expand their applications in optical or electronic areas.

Acknowledgements

This work was supported by the National Natural Science Foundation of China (20971100) and Program for New Century Excellent Talents in University (NCET-08-0398) and Developing Science Funds of Tongji University.

References

1 M. D. McGehee, T. Bergstedt, C. Zhang, A. P. Saab, M. B. O'Regan, G. C. Bazan, V. I. Srdanov and A. J. Heeger, *Adv. Mater.*, 1999, **11**, 1349–1354; J. M. Lehn, *Angew. Chem.*, 1990, **102**, 1347–1362; J. M. Lehn, *Angew. Chem., Int. Ed. Engl.*, 1990, **29**, 1304–1319; C. Koeppen, S. Yamada, G. Jiang, A. F. Garito and L. R. Dalton, *J. Opt. Soc. Am. B*, 1997, **14**, 155–162; X. M. Guo, H. D. Guo, L. S. Fu, R. P. Deng, W. Chen, J. Feng, S. Dang and H. J. Zhang, *J. Phys. Chem. C*, 2009, **113**, 2603–2610.
2 D. J. Zhang, X. M. Wang, Z. A. Qiao, D. H. Tang, Y. L. Liu and Q. S. Huo, *J. Phys. Chem. C*, 2010, **114**, 12505–12510; G. F. DeSá, O. L. Malta, C. De Mello Donegá, A. M. Simas, R. L. Longo, P. A. Santa-Cruz and E. F. da Silva Jr., *Coord. Chem. Rev.*, 2000, **196**, 165–195; N. Sabbatini, M. Guardingli and J. M. Lehn, *Coord. Chem. Rev.*, 1993, **123**, 201–228; M. Q. Tan, Z. Q. Ye, G. L. Wang and J. L. Yuan, *Chem. Mater.*, 2004, **16**, 2494–2498; P. Escribano, B. Julián-López, J. Planelles-Aragó, E. Cordoncillo, B. Viana and C. Sanchez, *J. Mater. Chem.*, 2008, **18**, 23–40.
3 L. H. Wang, W. Wang, W. G. Zhang, E. T. Kang and W. Huang, *Chem. Mater.*, 2000, **12**, 2212–2218; L. D. Carlos and A. L. L. Videira, *Phys. Rev. B: Condens. Matter*, 1994, **49**, 11721–11728.
4 R. Van Deun, D. Moors, B. De Fré and K. Binnemans, *J. Mater. Chem.*, 2003, **13**, 1520–1522.
5 D. Sendor and U. Kynast, *Adv. Mater.*, 2002, **14**, 1570–1574; H. Maas, A. Currao and G. Calzaferri, *Angew. Chem., Int. Ed.*, 2002, **41**, 2495–2497; P. Minoofar, R. Hernandez, S. Chia, B. Dunn, J. I. Zink and A. C. Franville, *J. Am. Chem. Soc.*, 2002, **124**, 14388–14396.
6 Q. H. Xu, L. S. Li, X. S. Liu and R. R. Xu, *Chem. Mater.*, 2002, **14**, 549–555; M. H. Bartl, B. J. Scott, H. C. Huang, G. Wirnsberger, A. Popitsch, B. F. Chmelka and G. D. Stucky, *Chem. Commun.*, 2002, 2474–2475.
7 D. Y. Zhao, J. Y. Sun, Q. Z. Li and G. D. Stucky, *Chem. Mater.*, 2000, **12**, 275–279; D. Y. Zhao, Q. S. Huo, J. P. Feng, N. Melosh, G. H. Fredrickson, B. F. Chmelka and G. D. Stucky, *Science*, 1998, **279**, 548–552; J. Feng, H. J. Zhang, C. Y. Peng, J. B. Yu, R. P. Deng, L. N. Sun and X. M. Guo, *Microporous Mesoporous Mater.*, 2008, **113**, 402–410.
8 C. Y. Peng, H. J. Zhang, J. B. Yu, Q. G. Meng, L. S. Fu, H. R. Li, L. N. Sun and X. M. Guo, *J. Phys. Chem. B*, 2005, **109**, 15278–15287; L. S. Li, Y. Zhang, J. B. Yu, C. Y. Peng and H. J. Zhang, *J. Photochem. Photobiol., A*, 2008, **199**, 57–63; C. Y. Peng, H. J. Zhang, Q. G. Meng, H. R. Li, J. B. Yu, J. F. Guo and L. N. Sun, *Inorg. Chem. Commun.*, 2005, **8**, 440–443.
9 Y. Li, B. Yan and H. Yang, *J. Phys. Chem. C*, 2008, **112**, 3959–3968; B. Yan and Y. Li, *Dalton Trans.*, 2010, **39**, 1480–1487; Y. J. Li and B. Yan, *Inorg. Chem.*, 2009, **48**, 8276–8285; L. L. Kong, B. Yan and Y. Li, *J. Solid State Chem.*, 2009, **182**, 1631–1637; L. L. Kong, B. Yan and Y. Li, *J. Alloys Compd.*, 2009, **481**, 549–554; Y. J. Li, B. Yan and Y. Li, *Chem.–Asian J.*, 2010, **5**, 1642–1651; Y. J. Li, B. Yan and Y. Li, *Microporous Mesoporous Mater.*, 2010, **131**, 82–88; Y. J. Li, L. Wang and B. Yan, *J. Mater. Chem.*, 2011, **21**, 1130–1138.
10 C. Sanchez, B. Julian, P. Belleville and M. Popall, *J. Mater. Chem.*, 2005, **15**, 3559–3592; P. Wang, C. Klein, R. Humphry, S. Zakeeruddin and M. Grätzel, *J. Am. Chem. Soc.*, 2005, **127**, 808–809.
11 P. Liu, H. R. Li, Y. G. Wang, B. Y. Liu, W. J. Zhang, Y. J. Wang, W. D. Yan, H. J. Zhang and U. Schubert, *J. Mater. Chem.*, 2008, **18**, 735–737; H. R. Li, P. Liu, Y. G. Wang, L. Zhang, J. B. Yu, H. J. Zhang, B. Y. Liu and U. Schubert, *J. Phys. Chem. C*, 2009, **113**, 3945–3949.
12 K. Binnemans, P. Lenaerts, K. Driesen and C. Görller-Walrand, *J. Mater. Chem.*, 2004, **14**, 191–195.
13 J. B. Yu, H. J. Zhang, L. S. Fu, R. P. Deng, L. Zhou, H. R. Li, F. Y. Liu and H. L. Fu, *Inorg. Chem. Commun.*, 2003, **6**, 852–854.
14 Q. M. Wang and B. Yan, *J. Mater. Chem.*, 2004, **14**, 2450–2454.
15 H. P. Wang, Y. F. Ma, H. Tian, N. Tang, W. S. Liu, Q. Wang and Y. Tang, *Dalton Trans.*, 2010, **39**, 7485–7492.
16 M. Kruk and M. Jaroniec, *Chem. Mater.*, 2001, **13**, 3169–3183; W. H. Zhang, X. B. Lu, J. H. Xiu, Z. L. Hua, L. X. Zhang, M. Robertson, J. L. Shi, D. S. Yan and J. D. Holmes, *Adv. Funct. Mater.*, 2004, **14**, 544–552.
17 H. R. Li, J. Lin, H. J. Zhang, L. S. Fu, Q. G. Meng and S. B. Wang, *Chem. Mater.*, 2002, **14**, 3651–2655; P. C. R. Soares-Santos, H. I. S. Nogueira, V. Félix, M. G. B. Drew, R. A. Sá Ferreira, L. D. Carlos and T. Trindade, *Chem. Mater.*, 2003, **15**, 100–108.
18 L. N. Sun, H. J. Zhang, C. Y. Peng, J. B. Yu, Q. G. Meng, L. S. Fu, F. Y. Liu and X. M. Guo, *J. Phys. Chem. B*, 2006, **110**, 7249–7258.
19 E. Guillet, D. Imbert, R. Scopelliti and J. C. G. Bünzli, *Chem. Mater.*, 2004, **16**, 4063–4070; F. Renaud, C. Piguet, G. Bernardinelli, J. C. G. Bünzli and G. Hopfgartner, *Chem.–Eur. J.*, 1997, **3**, 1660–1667; W. Q. Fan, J. Feng, S. Y. Song, Y. Q. Lei, G. L. Zheng and H. J. Zhang, *Chem.–Eur. J.*, 2010, **16**, 1903–1910.
20 M. H. V. Werts, R. T. F. Jukes and J. W. Verhoeven, *Phys. Chem. Chem. Phys.*, 2002, **4**, 1542–1548; E. E. S. Teotonio, J. G. P. Espinola, H. F. Brito, O. L. Malta, S. F. Oliveria, D. L. A. de Faria and C. M. S. Izumi, *Polyhedron*, 2002, **21**, 1837–1844; L. D. Carlos, V. D. Bermudez, R. A. S. Ferreira, L. Marques and M. Assuncao, *Chem. Mater.*, 1999, **11**, 581–588; L. N. Sun, H. J. Zhang, C. Y. Peng, J. B. Yu, Q. G. Meng, L. S. Fu, F. Y. Liu and X. M. Guo, *J. Phys. Chem. B*, 2006, **110**, 7249–7258.
21 J. C. Boyer, F. Vetrone, J. A. Capobianco, A. Speghini and M. Bettinelli, *J. Phys. Chem. B*, 2004, **108**, 20137–20144.
22 H. R. Li, P. Liu, Y. G. Wang, L. Zhang, J. B. Yu, H. J. Zhang, B. Y. Liu and U. Schubert, *J. Phys. Chem. C*, 2009, **113**, 3945–3949.
23 R. M. Supkowski and W. D. Horrocks, *Inorg. Chim. Acta*, 2002, **340**, 44–48.
24 W. F. Krupke, *Phys. Rev.*, 1966, **145**, 325–327.
25 Y. S. Liu, W. Q. Luo, R. F. Li, G. K. Liu, M. R. Antonio and X. Y. Chen, *J. Phys. Chem. C*, 2008, **112**, 686–694.
26 Q. B. Xiao, Y. S. Liu, L. Q. Liu, R. F. Li, W. Q. Luo and X. Y. Chen, *J. Phys. Chem. C*, 2010, **114**, 9314–932.

